Technical Report (draft)

Extension of Bicoherence Analysis to Multivariate Domains with Application to AstroGK Data

For Plasma Physics Laboratory — Koepke (PPL-K)

𝔾. 𝔸. ℝiggs — ©2023 WVU

Contents

1 Derivation of vector bispectrum

Consider some real-valued, integrable function $f : \mathbb{R}^3 \to \mathbb{R}$. In analogy to the scalar case, the triple (auto-)correlation is given by

$$C(\boldsymbol{r}_1, \boldsymbol{r}_2) = \int_{\mathbb{R}^3} d^3\zeta \, f(\boldsymbol{\zeta}) f(\boldsymbol{\zeta} + \boldsymbol{r}_1) f(\boldsymbol{\zeta} + \boldsymbol{r}_2). \tag{1}$$

In three dimensions, the Fourier transform and its inverse are

$$\mathcal{F}\left\{f(\boldsymbol{r}')\right\} \equiv \hat{f}(\boldsymbol{k}) = \int_{\mathbb{R}^3} d^3r \, f(\boldsymbol{r}) e^{-i\boldsymbol{k}\cdot\boldsymbol{r}}, \tag{2}$$

$$\mathcal{F}^{-1}\left\{\hat{f}(\boldsymbol{k}')\right\} = f(\boldsymbol{r}) = \frac{1}{(2\pi)^3} \int_{\mathbb{R}^3} d^3k \, \hat{f}(\boldsymbol{k}) e^{i\boldsymbol{k}\cdot\boldsymbol{r}}. \tag{3}$$

Thus, we may write (1) as

$$C(\boldsymbol{r}_1, \boldsymbol{r}_2) = \frac{1}{(2\pi)^6} \int_{\mathbb{R}^3} d^3\zeta \, f(\boldsymbol{\zeta}) \int_{\mathbb{R}^3} d^3k_1 \, \hat{f}(\boldsymbol{k}_1) e^{i\boldsymbol{k}_1\cdot(\boldsymbol{\zeta}+\boldsymbol{r}_1)} \int_{\mathbb{R}^3} d^3k_2 \, \hat{f}(\boldsymbol{k}_2) e^{i\boldsymbol{k}_2\cdot(\boldsymbol{\zeta}+\boldsymbol{r}_2)}. \tag{4}$$

As in the scalar case, we shuffle the order of integration (f is integrable by definition), finding that

$$C(\boldsymbol{r}_1, \boldsymbol{r}_2) = \frac{1}{(2\pi)^6} \int_{\mathbb{R}^3} d^3k_1 \int_{\mathbb{R}^3} d^3k_2 \, \hat{f}(\boldsymbol{k}_1) \hat{f}(\boldsymbol{k}_2) e^{i\boldsymbol{k}_1\cdot\boldsymbol{r}_1 + i\boldsymbol{k}_2\cdot\boldsymbol{r}_2} \int_{\mathbb{R}^3} d^3\zeta \, f(\boldsymbol{\zeta}) e^{i(\boldsymbol{k}_1+\boldsymbol{k}_2)\cdot\boldsymbol{\zeta}}. \tag{5}$$

Because $f \in \mathbb{R}$, the innermost integral is nothing but the complex conjugate of $\hat{f}(\boldsymbol{k}_1 + \boldsymbol{k}_2)$, leaving

$$C(\boldsymbol{r}_1, \boldsymbol{r}_2) = \frac{1}{(2\pi)^6} \int_{\mathbb{R}^3} d^3k_1 \int_{\mathbb{R}^3} d^3k_2 \, \hat{f}(\boldsymbol{k}_1) \hat{f}(\boldsymbol{k}_2) \overline{\hat{f}(\boldsymbol{k}_1 + \boldsymbol{k}_2)} e^{i\boldsymbol{k}_1\cdot\boldsymbol{r}_1 + i\boldsymbol{k}_2\cdot\boldsymbol{r}_2}, \tag{6}$$

which we immediately recognize as a six-dimensional inverse Fourier transform,

$$C(\boldsymbol{r}_1, \boldsymbol{r}_2) = \mathcal{F}^{-1}\left\{\hat{f}(\boldsymbol{k}_1) \hat{f}(\boldsymbol{k}_2) \overline{\hat{f}(\boldsymbol{k}_1 + \boldsymbol{k}_2)}\right\}. \tag{7}$$

Hence, our well-developed intuition for bicoherence analysis carries over to the vector-valued case. Performing an ensemble average (w.r.t. an arbitrary parameter τ) of the quantity in braces yields the bispectrum,

$$\boxed{\mathcal{B}(\boldsymbol{k}_1, \boldsymbol{k}_2) = \left\langle \hat{f}(\boldsymbol{k}_1) \hat{f}(\boldsymbol{k}_2) \overline{\hat{f}(\boldsymbol{k}_1 + \boldsymbol{k}_2)} \right\rangle_\tau} \equiv \frac{1}{\tau_f - \tau_i} \int_{\tau_i}^{\tau_f} d\tau \hat{f}(\boldsymbol{k}_1) \hat{f}(\boldsymbol{k}_2) \overline{\hat{f}(\boldsymbol{k}_1 + \boldsymbol{k}_2)}. \tag{8}$$

where here, $f = f(\boldsymbol{r}, \tau) \to \hat{f}(\boldsymbol{k}, \tau)$. The squared bicoherence spectrum is then easily defined as

$$\boxed{b^2(\boldsymbol{k}_1, \boldsymbol{k}_2) = \frac{|\mathcal{B}(\boldsymbol{k}_1, \boldsymbol{k}_2)|^2}{\left\langle \left| \hat{f}(\boldsymbol{k}_1) \hat{f}(\boldsymbol{k}_2) \right|^2 \right\rangle_\tau \left\langle \left| \hat{f}\left(\boldsymbol{k}_1 + \boldsymbol{k}_2\right) \right|^2 \right\rangle_\tau}}. \tag{9}$$

2 Notes from 13 April, 2023

2.1 AstroGK data

After a small amount of post-processing, the simulation's output is given in the mixed form,

$$\widehat{\mathbf{B}}(\boldsymbol{k}) \equiv \widehat{\mathbf{B}}(k_x, k_y, z, t) = \int_{\mathbb{R}} dx \int_{\mathbb{R}} dy \, \mathbf{B}(x, y, z, t) e^{-i(k_x x + k_y y)}, \tag{10}$$

where $\boldsymbol{k} = k_x \widehat{\boldsymbol{x}} + k_y \widehat{\boldsymbol{y}}$, and $\mathbf{B} = \delta\mathbf{B}$ is the magnetic field fluctuation. Figures 1 & 2 depict the development of $B_x(x, y, z = 0, t)$ and $B_y(x, y, z = 0, t)$ across six instants of time.

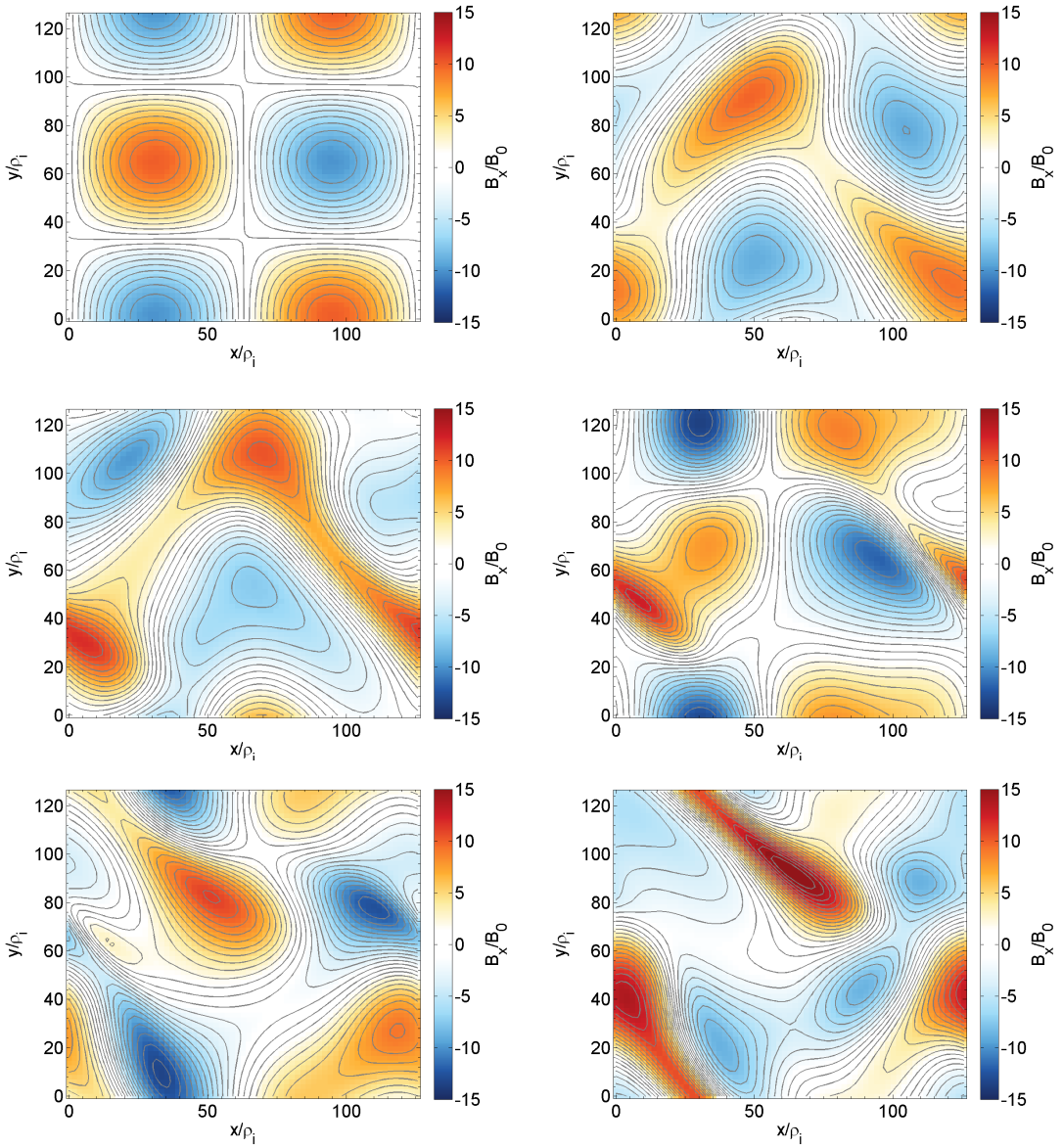

Figure 1: Evolution of x-component of magnetic field fluctuation for timestep $n_t = 2,101$ [*row #1*], $n_t = 201,301$ [*row #2*], and $n_t = 401,501$ [*row #3*]. Note that we have assumed the same parameters as used in Howes (2016), thus $L_x = L_y = 40\pi\rho_i$.

2.2 Alfvén wave collisions

We first write the incompressible MHD equations in Elsässer form, as in Howes and Nielson (2013) & Howes (2016),

$$\frac{\partial \boldsymbol{z}^{\pm}}{\partial t} \mp (\boldsymbol{v}_A \cdot \nabla)\boldsymbol{z}^{\pm} = -(\boldsymbol{z}^{\pm} \cdot \nabla)\boldsymbol{z}^{\pm} - \nabla P/\rho_0, \tag{11}$$

where $\boldsymbol{z}^{\pm} \equiv \boldsymbol{u} \pm \delta\mathbf{B}/\sqrt{4\pi\rho_0}$ are Elsässer variables, $\boldsymbol{v}_A$ is the usual Alfvén velocity, and ρ_0 the mass density. Incompressibility is maintained by $\nabla \cdot \boldsymbol{z}^{\pm} = 0$. The relevant physics are contained

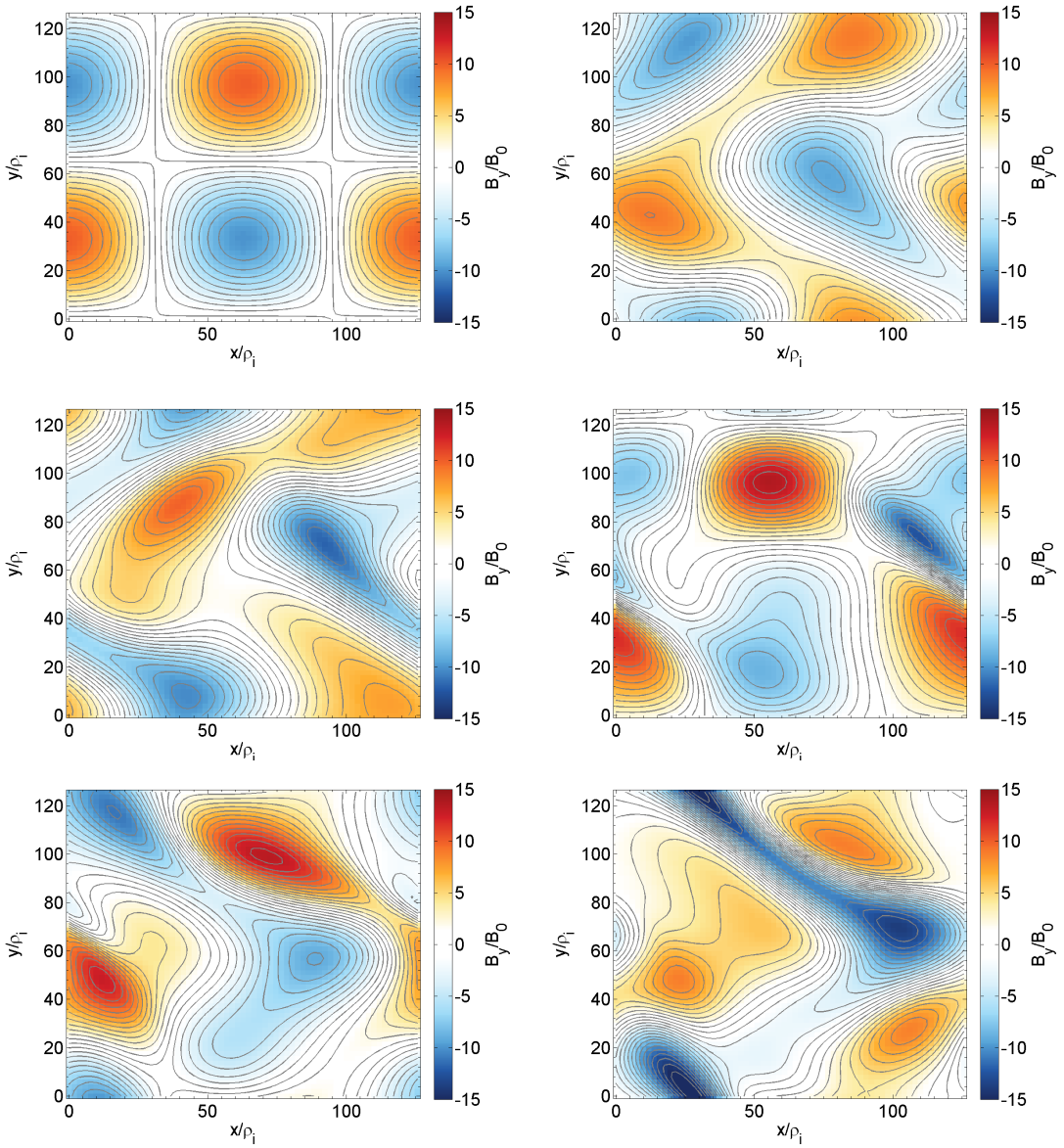

Figure 2: Evolution of y-component of magnetic field fluctuation for timestep $n_t = 2, 101$ [*row #1*], $n_t = 201, 301$ [*row #2*], and $n_t = 401, 501$ [*row #3*].

in the nonlinearity on the r.h.s.; for simplicity, we focus on the curvature term,

$$(\boldsymbol{z}^{\pm} \cdot \nabla)\boldsymbol{z}^{\pm} \to [\mathbf{B}(\boldsymbol{x}, z, t) \cdot \nabla]\, \mathbf{B}(\boldsymbol{x}, z, t), \tag{12}$$

applying the (slightly abusive) shorthand $\boldsymbol{x} = x\widehat{\boldsymbol{x}} + y\widehat{\boldsymbol{y}}$. Using (10), we see that

$$\begin{aligned} \mathbf{B}(\boldsymbol{x}, z, t) &= \frac{1}{(2\pi)^2} \int_{\mathbb{R}} dk_x \int_{\mathbb{R}} dk_y\, \widehat{\mathbf{B}}(k_x, k_y, z, t) e^{i(k_x x + k_y y)}, \\ &= \frac{1}{(2\pi)^2} \int_{\mathbb{R}^2} d^2k\, \widehat{\mathbf{B}}(\boldsymbol{k}) e^{i\boldsymbol{k}\cdot\boldsymbol{x}}. \end{aligned} \tag{13}$$

Therefore, (12) becomes

$$(\mathbf{B}\cdot\nabla)\,\mathbf{B} = \frac{1}{(2\pi)^4}\int d^2k_1 \int d^2k_2 \left[\widehat{\mathbf{B}}(\boldsymbol{k}_1)e^{i\boldsymbol{k}_1\cdot\boldsymbol{x}}\cdot i\boldsymbol{k}_2\right]\widehat{\mathbf{B}}(\boldsymbol{k}_2)e^{i\boldsymbol{k}_2\cdot\boldsymbol{x}}, \tag{14}$$

where we assume $\nabla \to \partial/\partial\boldsymbol{x}$. Expanding the integrand yields

$$\begin{aligned} i\left[\widehat{\mathbf{B}}(\boldsymbol{k}_1)\cdot\boldsymbol{k}_2\right]\widehat{\mathbf{B}}(\boldsymbol{k}_2)e^{i(\boldsymbol{k}_1+\boldsymbol{k}_2)\cdot\boldsymbol{x}} &= i\left[\widehat{B}_x(\boldsymbol{k}_1)k_{2x}+\widehat{B}_y(\boldsymbol{k}_1)k_{2y}\right]\left[\widehat{B}_x(\boldsymbol{k}_2)\widehat{\boldsymbol{x}}+\widehat{B}_y(\boldsymbol{k}_2)\widehat{\boldsymbol{y}}\right]e^{i(\boldsymbol{k}_1+\boldsymbol{k}_2)\cdot\boldsymbol{x}}, \\ &= i\Big\{\left[\widehat{B}_x(\boldsymbol{k}_1)k_{2x}\widehat{B}_x(\boldsymbol{k}_2)+\widehat{B}_y(\boldsymbol{k}_1)k_{2y}\widehat{B}_x(\boldsymbol{k}_2)\right]\widehat{\boldsymbol{x}} \\ &\quad +\left[\widehat{B}_x(\boldsymbol{k}_1)k_{2x}\widehat{B}_y(\boldsymbol{k}_2)+\widehat{B}_y(\boldsymbol{k}_1)k_{2y}\widehat{B}_y(\boldsymbol{k}_2)\right]\widehat{\boldsymbol{y}}\Big\}e^{i(\boldsymbol{k}_1+\boldsymbol{k}_2)\cdot\boldsymbol{x}}. \end{aligned} \tag{15}$$

3 Implementation

3.1 Code sketch

When $\boldsymbol{k}$ is two-dimensional, we see that (8) becomes

$$\mathcal{B}(k_{1x},k_{1y},k_{2x},k_{2y}) = \left\langle \hat{f}(k_{1x},k_{1y})\hat{f}(k_{2x},k_{2y})\overline{\hat{f}(k_{1x}+k_{2x},k_{1y}+k_{2y})}\right\rangle. \tag{16}$$

Hence, we use the following code to calculate the bispectrum and squared bicoherence spectrum:

```
function [B,e12,e3] = vec_bispec(f,N)
% Main cogwork of vector bispectral analysis
% f is (N x N) data slice

% Initialization
B = zeros(N,N,N,N);
e12 = zeros(N,N,N,N);
e3  = zeros(N,N,N,N);

% Do a loop^4
for k1x=1:N
  for k2x=1:N-k1x+1

    for k1y=1:N
      for k2y=1:N-k1y+1

        % Eliminate redundant peaks ;^]
        % ~> Swapping k1 & k2 shouldn't matter for auto-vector-bispectrum
        if (k1x-1)^2 + (k1y-1)^2 <= (k2x-1)^2 + (k2y-1)^2

            % Bispectrum
            B(k1y,k1x,k2y,k2x) = f(k1y,k1x) * f(k2y,k2x) ...
                               * conj( f(k1y+k2y-1,k1x+k2x-1) );
            % Normalizations for squared bicoherence spectrum
            e12(k1y,k1x,k2y,k2x) = abs( f(k1y,k1x) * f(k2y,k2x) )^2;
            e3(k1y,k1x,k2y,k2x)  = abs( f(k1y+k2y-1,k1x+k2x-1) )^2;

        end

      end
    end

  end
end
```

Because this is an auto-bispectral analysis, we avoid redundant peaks (due to the symmetry $\mathcal{B}(\boldsymbol{k}_1,\boldsymbol{k}_2) = \mathcal{B}(\boldsymbol{k}_2,\boldsymbol{k}_1)$) by first checking that $|\boldsymbol{k}_1| < |\boldsymbol{k}_2|$.

Then, we invoke `vec_bispec` for each term in the ensemble average,

```
function [B,b2] = calc_vec_bispec(f)
% Calculate bispectrum and bicoherence spectrum for data f
% f = (N x N x Nslice) array

% Small parameter for NaN prevention
lilguy = 1e-6;

% Get data params and initialize
[N,~,Nslice] = size(f);
B = zeros(N,N,N,N);
e12 = zeros(N,N,N,N);
e3  = zeros(N,N,N,N);

for j=1:Nslice
  fprintf(sprintf('Slice = %d/%d\n',j,Nslice));

  % Calculate bispectrum and expectations for each slice
  [B_i,e12_i,e3_i] = vec_bispec(f(:,:,j),N);

  % Sums
  B = B + B_i;
  e12 = e12 + e12_i;
  e3  = e3  + e3_i;

end
fprintf('\n')

% Bicoherence spectrum
b2 = abs(B).^2 ./ (e12 .* e3 + lilguy);
% Final bispectrum is simple average
B = B/Nslice;
```

For completeness, the discrete bispectrum and discrete squared bicoherence spectrum are then, respectively,

$$\begin{aligned} \mathcal{B}[m,n,p,q] &= \left\langle \hat{f}[m,n]\,\hat{f}[p,q]\,\overline{\hat{f}[m+p,n+q]} \right\rangle, \\ b^2[m,n,p,q] &= \frac{|\mathcal{B}[m,n,p,q]|^2}{\left\langle \left|\hat{f}[m,n]\hat{f}[p,q]\right|^2 \right\rangle \left\langle \left|\hat{f}\,[m+p,n+q]\right|^2 \right\rangle + \varepsilon}, \end{aligned} \quad \Big| \quad m+p, n+q \leq N, \tag{17}$$

where N is the dimension[1] of $\hat{f}$, and $\varepsilon \ll 1$ is a small number used to avoid evaluation of $0/0 = \mathrm{NaN}$.

3.2 Data visualization

Because we are innately ill-equipped to visualize four-dimensional data, we layer isosurfaces of either $|\mathcal{B}(\boldsymbol{k}_1, \boldsymbol{k}_2)|$ or $b^2(\boldsymbol{k}_1, \boldsymbol{k}_2)$ in 3D "slices" of the larger 4D space. In MATLAB, we use, *e.g.*,

```
    b2_slice = reshape(b2(:,:,k2y,:),N,N,N);  % Reshape array to 3D
    isosurface(b2_slice,0.9)                  % Find smallest isosurface
    alpha(0.35);                              % Set transparency
    hold on;                                  % Enable overplotting
    for j=1:8; isosurface(b2_slice,j/10); end % Layer isosurfaces
```

[1] We have been somewhat glib about restrictions on the matrix representation of $\hat{f}$, as the two-dimensional Fourier transform of real-valued data is symmetric about the Nyquist wavevector (if the original data f has size $M \times M$, then $k_{\mathrm{Nyq},1} = k_{\mathrm{Nyq},2} = \lfloor M/2 \rfloor$). Thus, we assume that all $\boldsymbol{k}$-spectra $\hat{f}$ considered in this report contain no spatial frequencies which exceed the Nyquist criterion.

4 Code validation

4.1 3 static modes

To begin convincing ourselves the code behaves as intended, we check the simplest diagnostic case. Explicitly, we consider the wavevectors

$$\begin{aligned} \boldsymbol{k}/k_\perp &= 6\widehat{\boldsymbol{x}} + 2\widehat{\boldsymbol{y}}, \\ \boldsymbol{k}'/k_\perp &= 4\widehat{\boldsymbol{x}} + 4\widehat{\boldsymbol{y}}, \\ \boldsymbol{k}'' &= \boldsymbol{k} + \boldsymbol{k}'. \end{aligned} \tag{18}$$

Since $|\boldsymbol{k}| > |\boldsymbol{k}'|$, we expect to find a single peak at $\mathcal{B}(k_{1x}/k_\perp, k_{1y}/k_\perp, k_{2x}/k_\perp, k_{2y}/k_\perp) = \mathcal{B}(4, 4, 6, 2)$. This is precisely what is observed in Fig. 3.

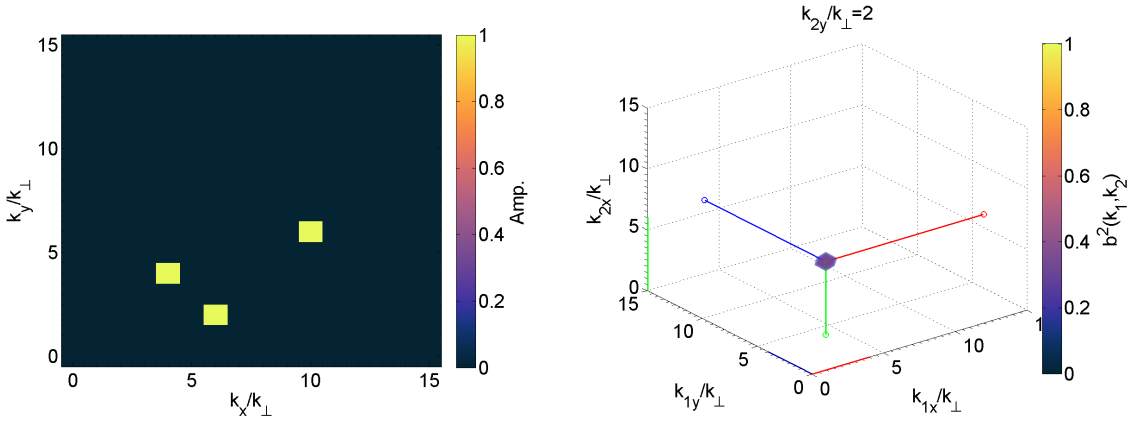

Figure 3: Visualization of diagnostic $\boldsymbol{k}$-space [*left*] with wavevectors given by (18). Plot of isosurfaces of squared bicoherence $b^2(\boldsymbol{k}_1, \boldsymbol{k}_2)$ [*right*] within the 3D "slice" $k_{2y}/k_\perp = 2$. Note that axes have been "painted" to aid identification of relevant coordinates, and maximum value of b^2 is likewise pinpointed.

4.2 Phase dynamics

Theory implies that the bispectrum should tend to vanish wherever its phase varies randomly (or linearly). Thus, by multiplying the static amplitudes in (18) by a random phasor for a number of realizations, we should null out the resulting bicoherence spectrum. A plot of the peak bicoherence vs. realization number is given in Fig. 4, confirming this hypothesis.

4.3 Time evolution

Next, we allow the coupled wavevectors to evolve in time as the averaging is performed. In particular, we have

$$\begin{aligned} \boldsymbol{k}/k_\perp &= (3+t)\widehat{\boldsymbol{y}}, \\ \boldsymbol{k}'/k_\perp &= (2+t)\widehat{\boldsymbol{x}}, \\ \boldsymbol{k}'' &= \boldsymbol{k} + \boldsymbol{k}', \end{aligned} \tag{19}$$

where the "time" t is stepped from 1 to 10, by unity. Our intuition from the scalar case tells us that all phase-coherent contributions to the final bispectrum will be retained, and thus we should find a swath of bicoherent features. Fortunately, Fig. 5 reports 10 individual peaks, each provided by a single interval of time.

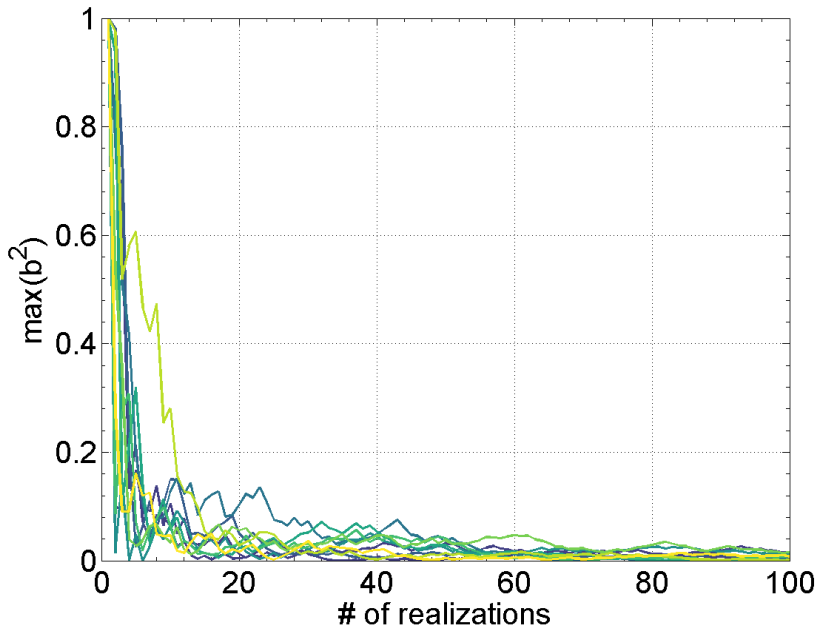

Figure 4: Plot of maximum value of squared bicoherence vs. number of randomized phases in the ensemble average, for 10 different runs. Note tendency of b^2 to approach zero as more incoherent fluctuations are averaged. Crucially, **this process may be used to deduce the noise floor, and therefore the uncertainty in** b^2.

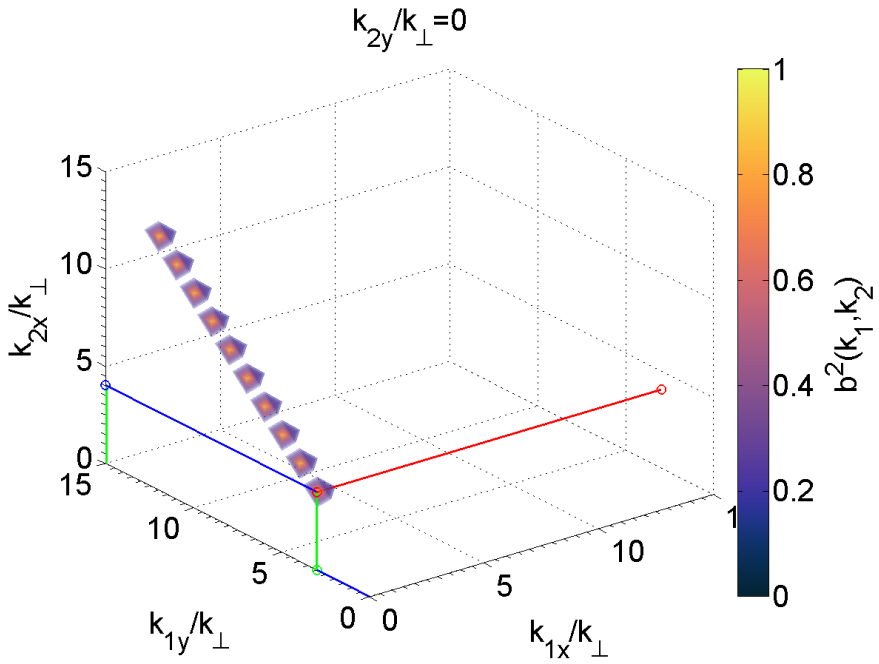

Figure 5: Isosurfaces of squared bicoherence $b^2(\boldsymbol{k}_1, \boldsymbol{k}_2)$ for time-dependent case. Note the conspicuous layers of semi-transparent isosurfaces enveloping the peaks.

4.4 Contrived bispectrum

Before moving on to more relevant examples, we pause to address a mildly artistic use of the bispectrum, akin to that given in §III.B of Riggs (2020). In particular, we create a simple "Flying WV" with a series of judiciously selected wavevectors (see Fig. 6). Each peak in the 4D $\mathcal{B}(\boldsymbol{k}_1, \boldsymbol{k}_2)$ is provided by a single interval of "time", and the color is determined by choosing the phase of $\hat{f}(\boldsymbol{k}_1 + \boldsymbol{k}_2)$. In short, we control the phase of the bispectrum, *i.e.*, the biphase,

$$\beta(\boldsymbol{k}_1, \boldsymbol{k}_2) = \tan^{-1}\left\{\frac{\mathrm{Im}\left[\mathcal{B}(\boldsymbol{k}_1, \boldsymbol{k}_2)\right]}{\mathrm{Re}\left[\mathcal{B}(\boldsymbol{k}_1, \boldsymbol{k}_2)\right]}\right\}. \tag{20}$$

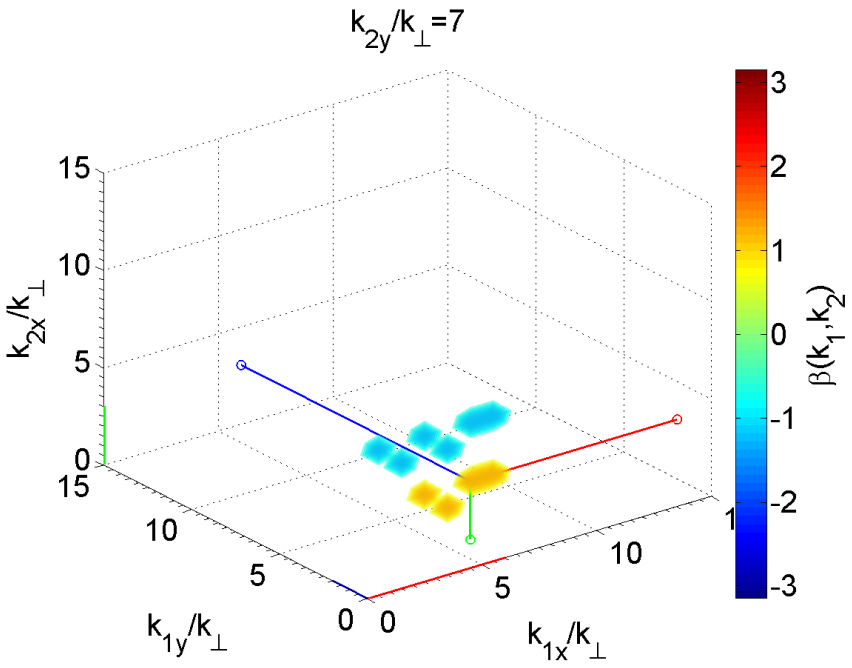

Figure 6: Isosurfaces of bispectrum $|\mathcal{B}(\boldsymbol{k}_1, \boldsymbol{k}_2)|$. Here, hue is determined by value of biphase $\beta(\boldsymbol{k}_1, \boldsymbol{k}_2)$.

4.5 Idealized nonlinear interaction

As a final check, we consider an analogue of the qualitative model given in Howes and Nielson (2013) & Howes (2016). To do so, we construct $\hat{f}(\boldsymbol{k})$ as a tridiagonal matrix, using

$$\hat{f}(k_x, k_y) = \begin{pmatrix} 0 & \epsilon & 0 & 0 & 0 & \dots \\ \epsilon & \epsilon^2 & \epsilon^3 & 0 & 0 & \dots \\ 0 & \epsilon^3 & \epsilon^4 & \epsilon^5 & 0 & \dots \\ 0 & 0 & \epsilon^5 & \epsilon^6 & \epsilon^7 & \dots \\ 0 & 0 & 0 & \epsilon^7 & \epsilon^8 & \dots \\ \vdots & \vdots & \vdots & \vdots & \vdots & \ddots \end{pmatrix}. \tag{21}$$

For simplicity, we restrict ourselves to constant values of amplitude ϵ. Figures 7–11 document the evolution of (21) and $b^2(\boldsymbol{k}_1, \boldsymbol{k}_2)$ for $\epsilon = [0.2, 0.4, 0.6, 0.8]$; results are summarized in Table 1. Roughly speaking, we observe enhanced nonlinear interaction as ϵ is increased.

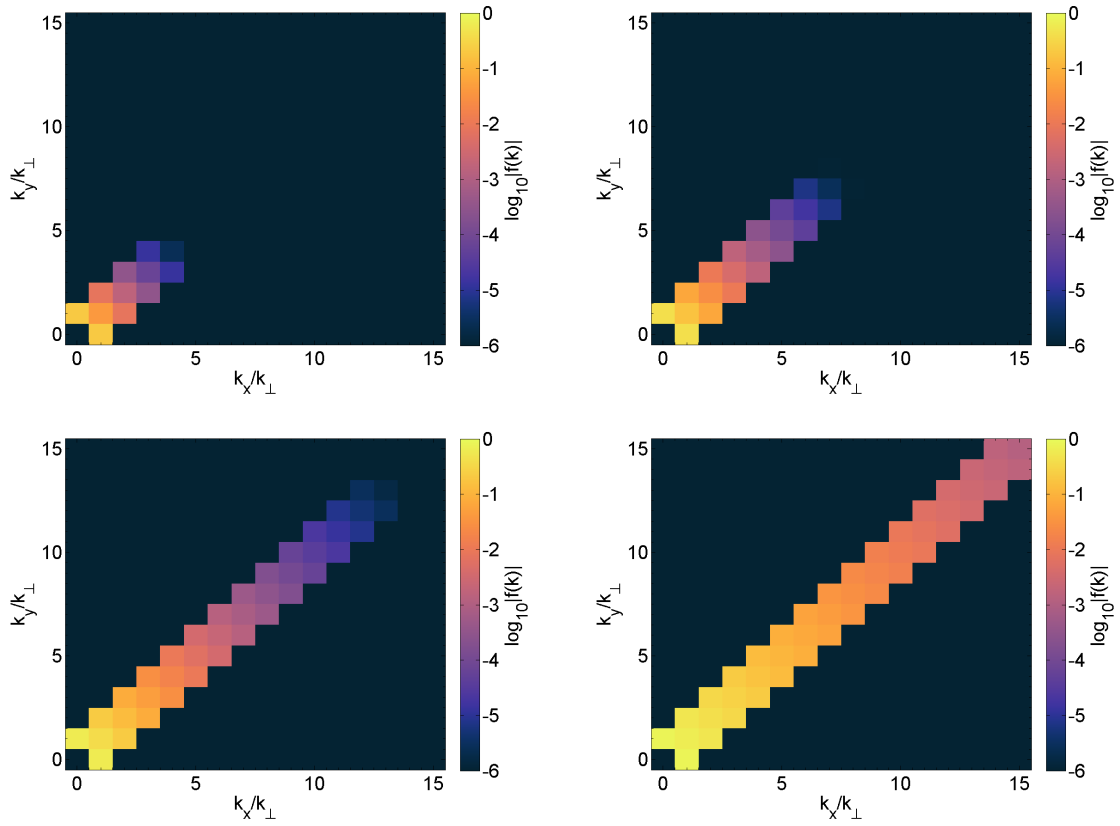

Figure 7: Visualization of considered $\boldsymbol{k}$-space for amplitude $\epsilon = 0.2$ [*upper left*], $\epsilon = 0.4$ [*upper right*], $\epsilon = 0.6$ [*bottom left*], and $\epsilon = 0.8$ [*bottom right*]. Note logarithmic color axis.

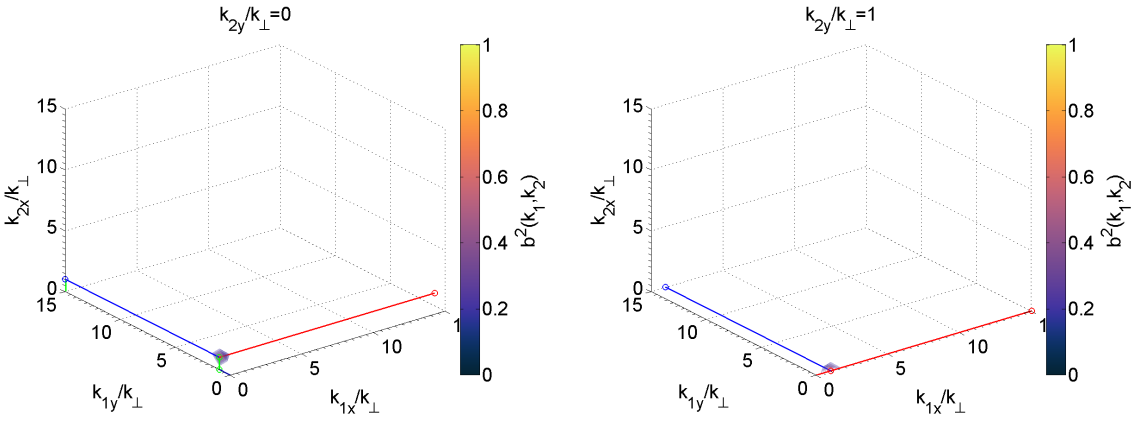

Figure 8: Isosurfaces of squared bicoherence $b^2(\boldsymbol{k}_1, \boldsymbol{k}_2)$ for $\epsilon = 0.2$. As before, all 3D slices of $k_{2y}/k_\perp$ containing statistically significant squared bicoherence ($b^2 \geq 0.1$) have been plotted. Specifically, this analysis infers nonlinear coupling between $\boldsymbol{k}/k_\perp = \widehat{\boldsymbol{x}}$ and $\boldsymbol{k}'/k_\perp = \widehat{\boldsymbol{y}}$. Note that both $k_{2y}/k_\perp = 0$ and $k_{2y}/k_\perp = 1$ implicate the same nonlinear interaction, as $b^2(0,1,1,0) = b^2(1,0,0,1) \approx 0.7$.

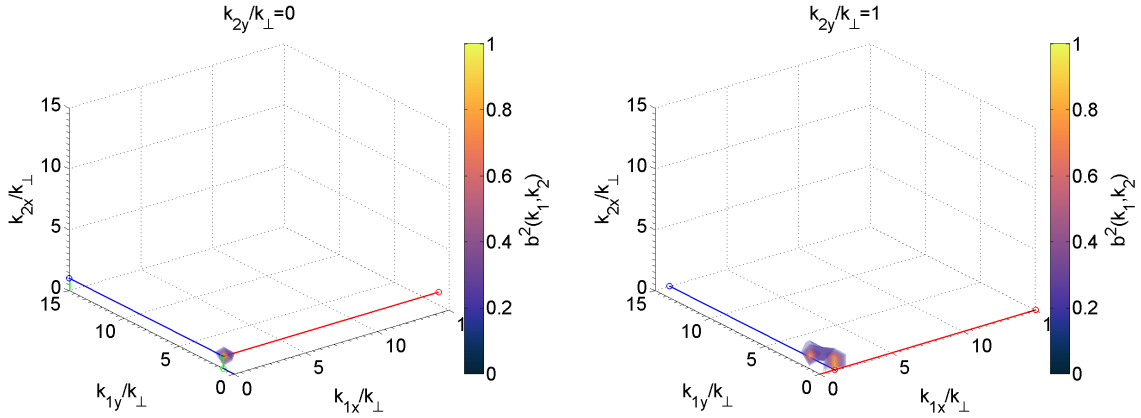

Figure 9: Isosurfaces of squared bicoherence $b^2(\boldsymbol{k}_1, \boldsymbol{k}_2)$ for $\epsilon = 0.4$ and $k_{2y}/k_\perp = [0, 1]$. Peaks representing significant nonlinear interaction ($b^2 \sim 1$) found at $b^2(0, 1, 1, 0) = b^2(1, 0, 0, 1)$, $b^2(0, 1, 1, 1)$, and $b^2(1, 0, 1, 1)$; weaker coupling ($b^2 \sim 0.3$) observed at $b^2(1, 1, 1, 1)$, $b^2(1, 0, 1, 2)$, and $b^2(0, 1, 2, 1)$; less significant coupling ($b^2 < 0.1$) located at $b^2(1, 1, 1, 2)$ and elsewhere.

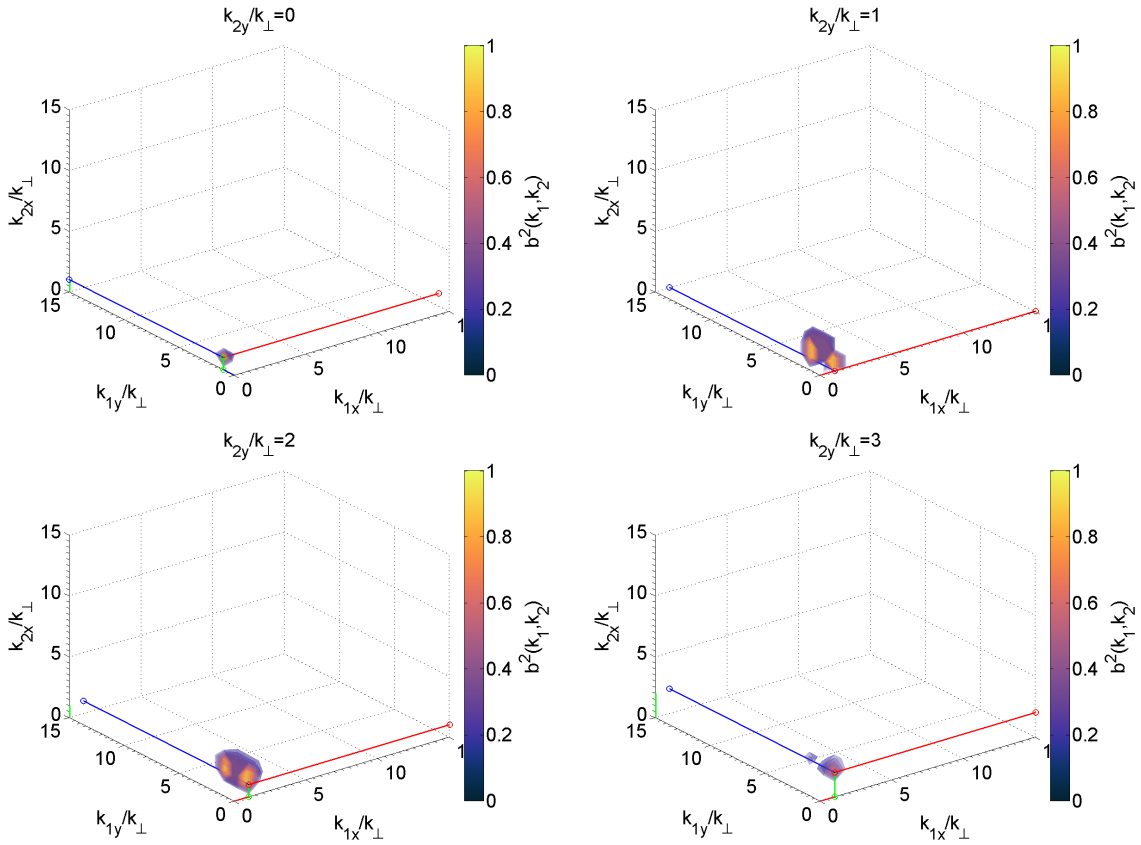

Figure 10: Isosurfaces of squared bicoherence $b^2(\boldsymbol{k}_1, \boldsymbol{k}_2)$ for $\epsilon = 0.6$ and $k_{2y}/k_\perp = [0, 3]$. The couplings observed in Figs. 8 & 9 remain, with new peaks appearing at $b^2(1, 1, 1, 2)$, $b^2(1, 1, 2, 1)$, etc. See Table 1 for more comprehensive information.

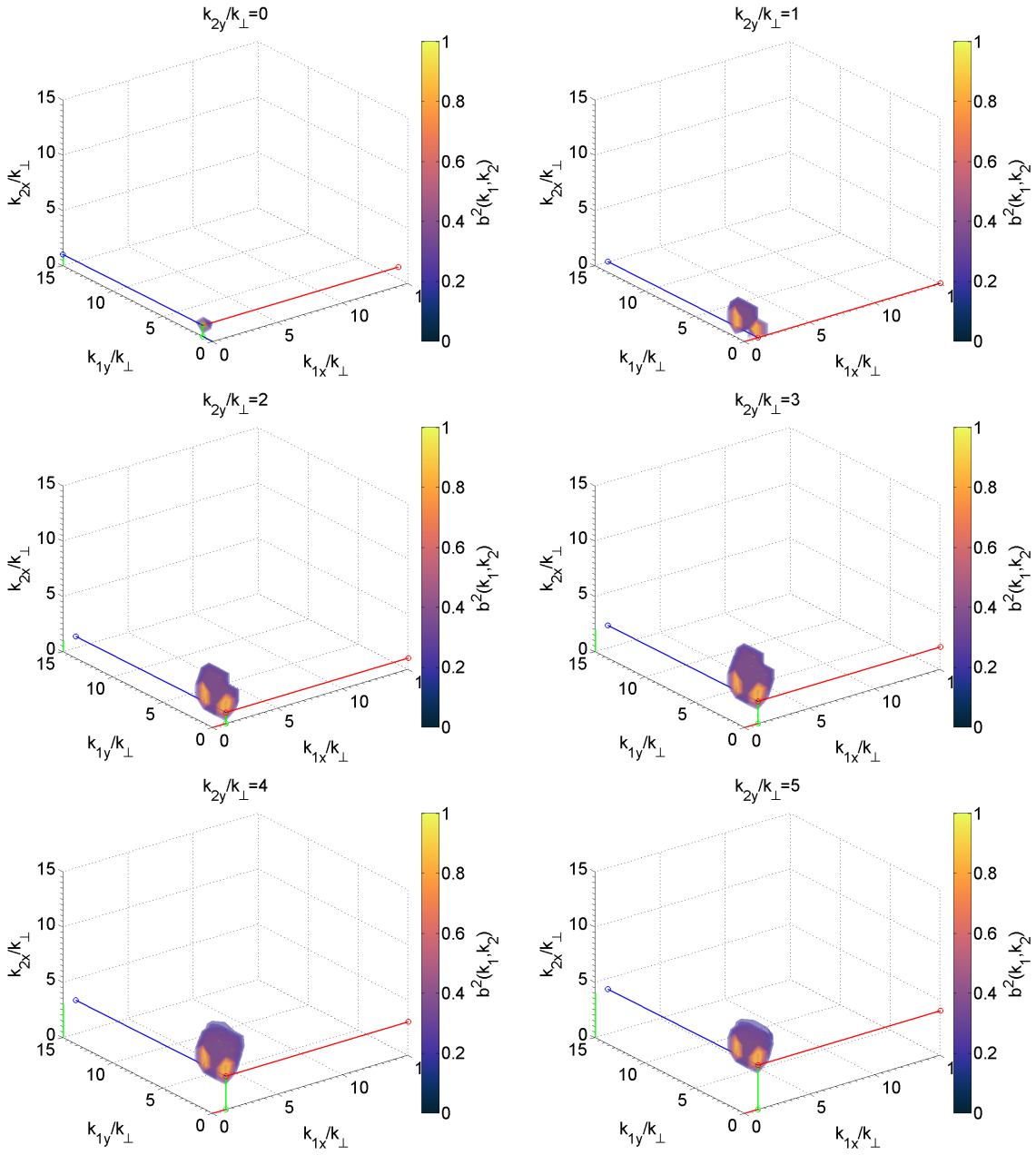

Figure 11: Isosurfaces of squared bicoherence $b^2(\boldsymbol{k}_1, \boldsymbol{k}_2)$ for $\epsilon = 0.8$ and $k_{2y}/k_\perp = [0, 5]$. Dozens of significant nonlinear couplings have been detected; see Table 1 for details.

ϵ	$(k_{1x}, k_{1y}, k_{2x}, k_{2y})$	$\boldsymbol{k}_1 + \boldsymbol{k}_2$	$b^2(\boldsymbol{k}_1, \boldsymbol{k}_2)$
0.2	(1,0,0,1)	(1,1)	0.719
	(0,1,1,0)	(1,1)	0.719
0.4	(1,0,0,1)	(1,1)	0.998
	(0,1,1,0)	(1,1)	0.998
	(0,1,1,1)	(1,2)	0.944
	(1,0,1,1)	(2,1)	0.944
	(1,1,1,1)	(2,2)	0.300
	(1,0,1,2)	(2,2)	0.300
	(0,1,2,1)	(2,2)	0.300
0.6	(1,0,0,1)	(1,1)	1.000
	(0,1,1,0)	(1,1)	1.000
	(0,1,1,1)	(1,2)	1.000
	(1,0,1,1)	(2,1)	1.000
	(1,1,1,1)	(2,2)	0.996
	(1,0,1,2)	(2,2)	0.996
	(0,1,2,1)	(2,2)	0.996
	(1,1,1,2)	(2,3)	0.973
	(1,1,2,1)	(3,2)	0.973
	(0,1,2,2)	(2,3)	0.973
	(1,0,2,2)	(3,2)	0.973
	(1,1,2,2)	(3,3)	0.826
	(2,1,1,2)	(3,3)	0.826
	(1,2,2,1)	(3,3)	0.826
	(1,0,2,3)	(3,3)	0.826
	(0,1,3,2)	(3,3)	0.826
	(1,2,2,2)	(3,4)	0.380
	(2,1,2,2)	(4,3)	0.380
	(1,1,2,3)	(3,4)	0.380
	(1,1,3,2)	(4,3)	0.380
0.8	(1,0,0,1)	(1,1)	1.000
	(0,1,1,0)	(1,1)	1.000
	(0,1,1,1)	(1,2)	1.000
	(1,0,1,1)	(2,1)	1.000
	(1,1,1,1)	(2,2)	1.000
	(1,0,1,2)	(2,2)	1.000
	(0,1,2,1)	(2,2)	1.000
	(1,1,1,2)	(2,3)	1.000
	(1,1,2,1)	(3,2)	1.000
	(0,1,2,2)	(2,3)	1.000
	(1,0,2,2)	(3,2)	1.000
	(1,1,2,2)	(3,3)	1.000
	(2,1,1,2)	(3,3)	1.000
	(1,2,2,1)	(3,3)	1.000
	(1,0,2,3)	(3,3)	1.000
	(0,1,3,2)	(3,3)	1.000
	(1,2,2,2)	(3,4)	0.999
	(2,1,2,2)	(4,3)	0.999
	(1,1,2,3)	(3,4)	0.999
	(1,1,3,2)	(4,3)	0.999

Table 1: Statistically significant ($b^2 \geq 0.1$) values of squared bicoherence for $\epsilon = [0.2, 0.4, 0.6, 0.8]$. Note that code output was limited to 20 peaks.

5 Analysis of AstroGK data

With newfound trust in our ability to produce vector bispectra, we (finally!) address the original purpose of this report.

5.1 Auto-bicoherence of B_x

Figure 1 visualizes the Fourier-transformed magnetic field $\widehat{B}_x(\boldsymbol{k}, z = 0, t)$ over six intervals of time. Assessment of auto-bicoherence is given in Table 2 and Figs. 13–14.

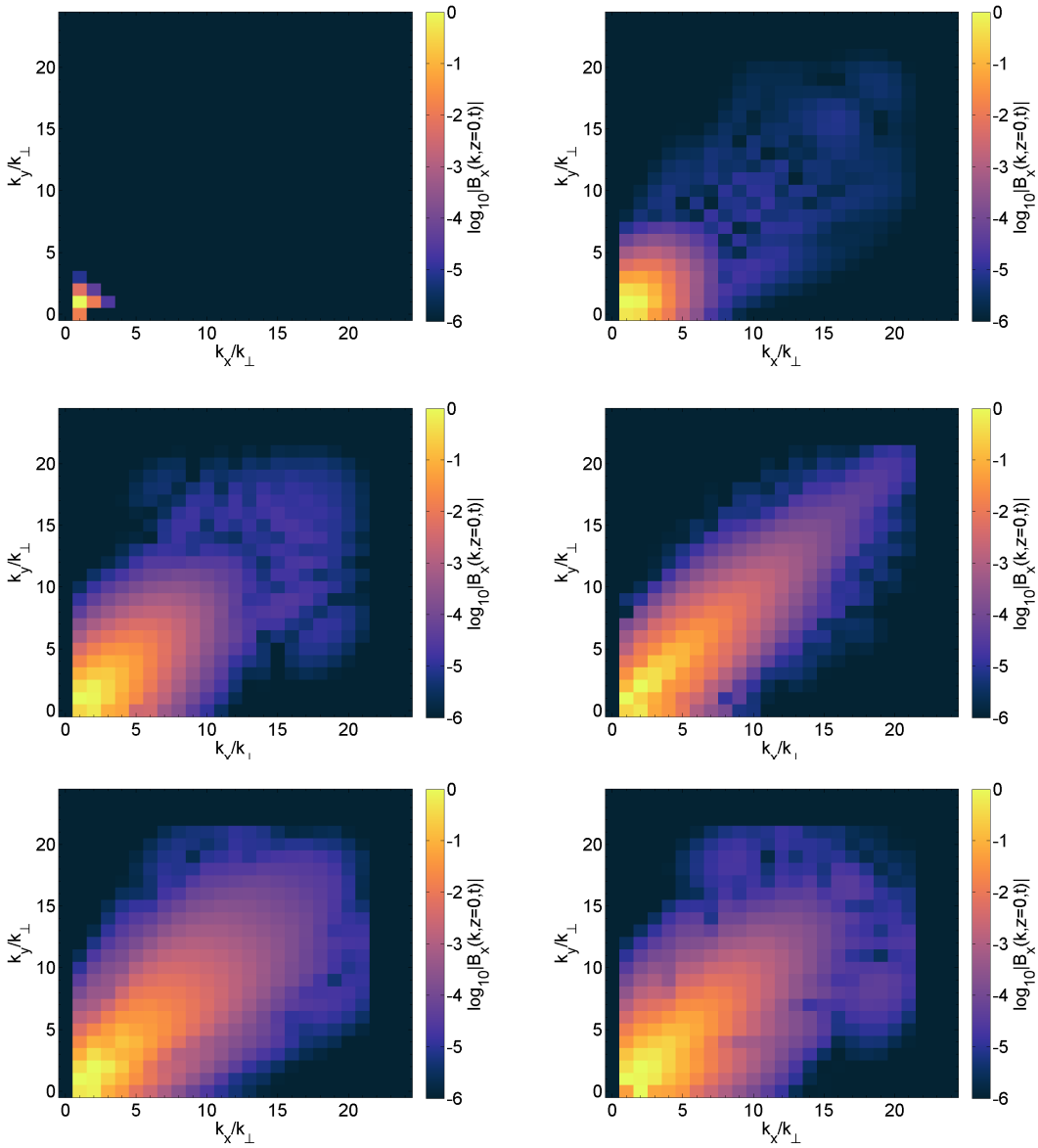

Figure 12: Evolution of $|\widehat{B}_x(\boldsymbol{k})|$ for timestep $n_t = 2,101$ [*row #1*], $n_t = 201,301$ [*row #2*], and $n_t = 401,501$ [*row #3*]. Note logarithmic color axis, and limitation to $k_x, k_y \leq 24k_\perp$.

timesteps	$(k_{1x}, k_{1y}, k_{2x}, k_{2y})$	$\boldsymbol{k}_1 + \boldsymbol{k}_2$	$b^2(\boldsymbol{k}_1, \boldsymbol{k}_2)$
[1,101]	(2,0,1,2)	(3,2)	0.999
	(2,0,2,2)	(4,2)	0.996
	(2,0,2,0)	(4,0)	0.988
	(2,0,1,3)	(3,3)	0.985
	(2,0,2,1)	(4,1)	0.975
	(1,1,2,0)	(3,1)	0.965
	(1,0,2,0)	(3,0)	0.964
	(1,0,1,3)	(2,3)	0.964
	(1,0,3,2)	(4,2)	0.962
	(1,0,2,3)	(3,3)	0.961
	(1,0,1,2)	(2,2)	0.961
	(1,0,2,2)	(3,2)	0.954
	(1,0,3,1)	(4,1)	0.948
	(1,0,2,1)	(3,1)	0.935
	(1,1,3,0)	(4,1)	0.930
	(1,0,1,1)	(2,1)	0.920
[101,201]	(2,0,4,4)	(6,4)	0.970
	(2,0,3,3)	(5,3)	0.965
	(1,1,5,2)	(6,3)	0.965
	(2,0,2,3)	(4,3)	0.964
	(2,0,4,3)	(6,3)	0.963
	(2,0,3,4)	(5,4)	0.961
	(2,2,4,2)	(6,4)	0.959
	(2,0,1,2)	(3,2)	0.955
	(1,1,5,5)	(6,6)	0.954
	(1,1,5,4)	(6,5)	0.954
	(1,1,4,5)	(5,6)	0.952
	(2,0,4,1)	(6,1)	0.951
	(1,1,4,2)	(5,3)	0.951
	(2,2,2,4)	(4,6)	0.951
	(1,1,2,4)	(3,5)	0.951
	(1,1,5,3)	(6,4)	0.949
[201,301]	(2,1,3,0)	(5,1)	0.983
	(1,0,2,2)	(3,2)	0.975
	(2,2,4,4)	(6,6)	0.971
	(3,0,2,3)	(5,3)	0.970
	(2,2,5,5)	(7,7)	0.970
	(3,0,3,4)	(6,4)	0.968
	(2,2,5,2)	(7,4)	0.967
	(1,0,5,5)	(6,5)	0.967
	(1,0,4,4)	(5,4)	0.966
	(3,3,4,4)	(7,7)	0.966
	(2,2,6,6)	(8,8)	0.966
	(1,0,3,3)	(4,3)	0.965
	(3,0,3,2)	(6,2)	0.965
	(1,0,6,6)	(7,6)	0.965
	(2,2,6,3)	(8,5)	0.964
	(2,2,3,3)	(5,5)	0.964

timesteps	$(k_{1x}, k_{1y}, k_{2x}, k_{2y})$	$\boldsymbol{k}_1 + \boldsymbol{k}_2$	$b^2(\boldsymbol{k}_1, \boldsymbol{k}_2)$
[301,401]	(2,2,5,4)	(7,6)	0.998
	(2,2,4,5)	(6,7)	0.998
	(2,2,6,6)	(8,8)	0.997
	(2,2,7,6)	(9,8)	0.996
	(2,2,6,7)	(8,9)	0.995
	(2,2,6,5)	(8,7)	0.995
	(2,2,5,5)	(7,7)	0.995
	(2,2,5,6)	(7,8)	0.995
	(2,2,4,4)	(6,6)	0.995
	(2,2,6,4)	(8,6)	0.994
	(2,2,7,7)	(9,9)	0.994
	(2,2,4,6)	(6,8)	0.994
	(2,2,3,2)	(5,4)	0.990
	(2,2,2,3)	(4,5)	0.990
	(2,2,7,5)	(9,7)	0.990
	(3,2,3,2)	(6,4)	0.988
[401,501]	(2,2,2,2)	(4,4)	0.991
	(2,0,1,2)	(3,2)	0.990
	(2,2,4,4)	(6,6)	0.982
	(1,2,4,2)	(5,4)	0.981
	(2,1,2,4)	(4,5)	0.981
	(2,0,2,4)	(4,4)	0.980
	(2,0,3,2)	(5,2)	0.979
	(2,0,4,1)	(6,1)	0.977
	(2,0,4,7)	(6,7)	0.975
	(2,2,4,0)	(6,2)	0.974
	(2,2,3,2)	(5,4)	0.972
	(2,2,2,3)	(4,5)	0.972
	(2,0,3,1)	(5,1)	0.971
	(2,2,5,3)	(7,5)	0.962
	(2,0,2,2)	(4,2)	0.961
	(2,2,3,5)	(5,7)	0.961
[1,501]	(2,2,7,7)	(9,9)	0.957
	(2,2,2,2)	(4,4)	0.948
	(2,2,8,7)	(10,9)	0.947
	(2,2,6,6)	(8,8)	0.944
	(2,2,7,8)	(9,10)	0.942
	(2,2,8,8)	(10,10)	0.939
	(2,2,6,5)	(8,7)	0.938
	(2,2,5,6)	(7,8)	0.938
	(2,2,4,4)	(6,6)	0.938
	(2,2,7,6)	(9,8)	0.936
	(2,2,6,7)	(8,9)	0.935
	(2,2,5,5)	(7,7)	0.929
	(2,2,7,5)	(9,7)	0.917
	(2,2,5,7)	(7,9)	0.916
	(2,2,5,4)	(7,6)	0.909
	(2,2,4,5)	(6,7)	0.909

Table 2: Greatest 16 values of squared auto-bicoherence $b^2(\boldsymbol{k}_1, \boldsymbol{k}_2)$ over six intervals of AstroGK output, for $B_x(x, y, z = 0, t)$

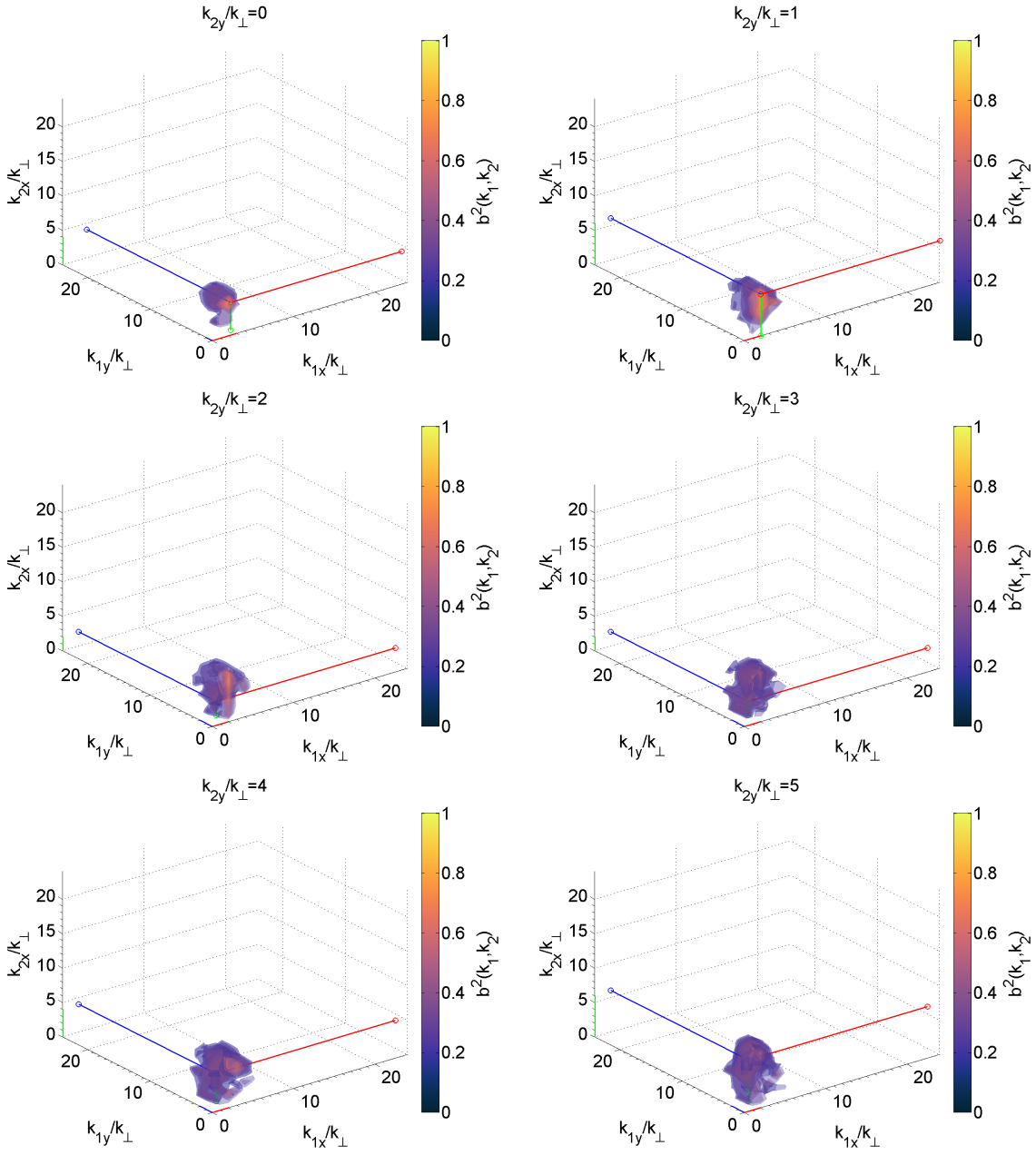

Figure 13: Isosurfaces of squared bicoherence $b^2(\boldsymbol{k}_1, \boldsymbol{k}_2)$ for $n_t = [1, 501]$ and $k_{2y}/k_\perp = [0, 5]$. Note that most peaks involve $\boldsymbol{k}/k_\perp = (2, 2)$; more detailed information is given in Table 2.

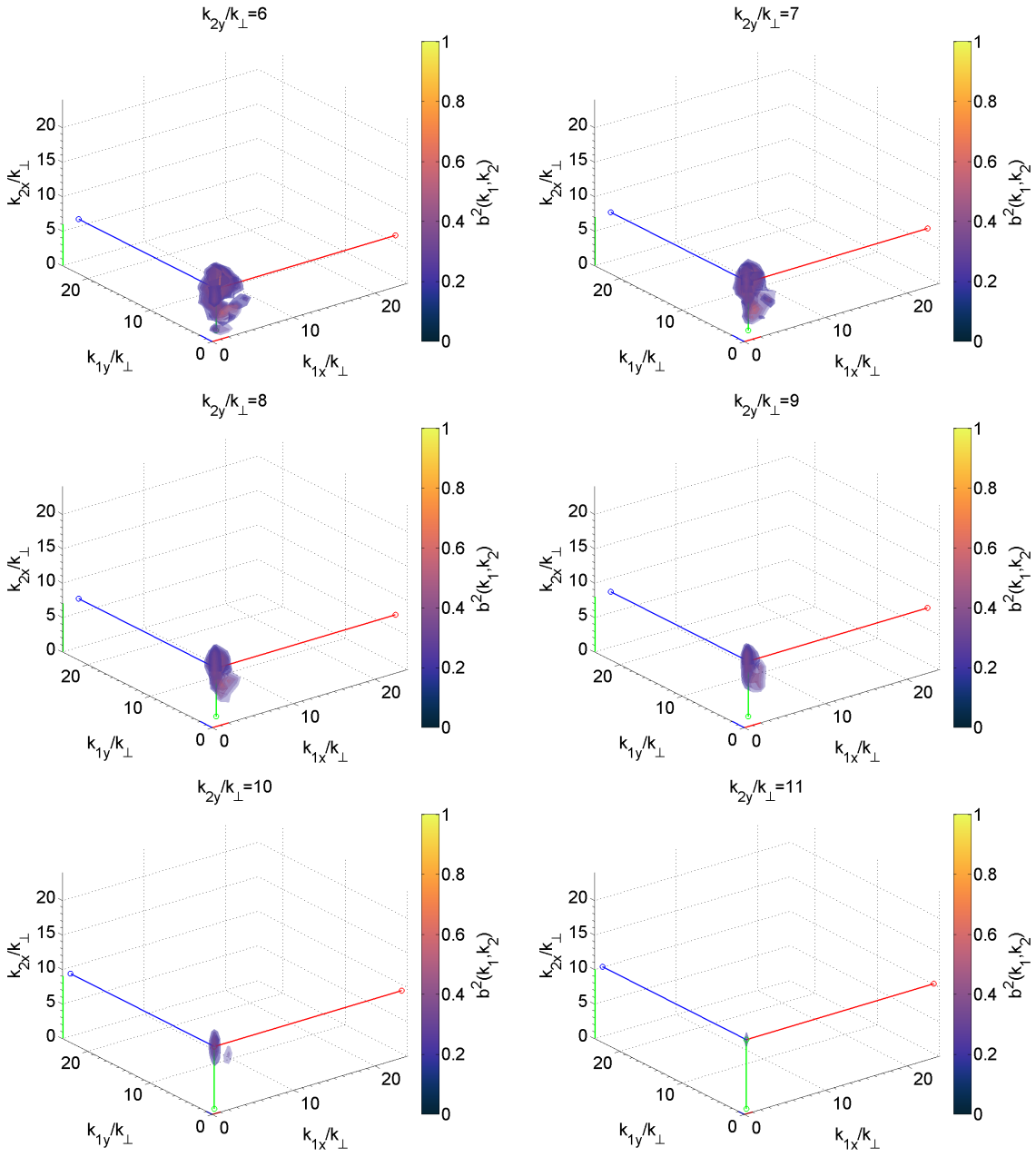

Figure 14: Isosurfaces of squared bicoherence $b^2(\boldsymbol{k}_1, \boldsymbol{k}_2)$ for $n_t = [1, 501]$ and $k_{2y}/k_\perp = [6, 11]$. Note again the appearance of $\boldsymbol{k}/k_\perp = (2, 2)$; see Table 2 for more information.

5.2 Auto-bicoherence of B_y

Figure 15 visualizes the Fourier-transformed magnetic field $\widehat{B}_y(\boldsymbol{k}, z = 0, t)$ over six intervals of time. Assessment of auto-bicoherence is given in Table 3 and Figs. 16–17.

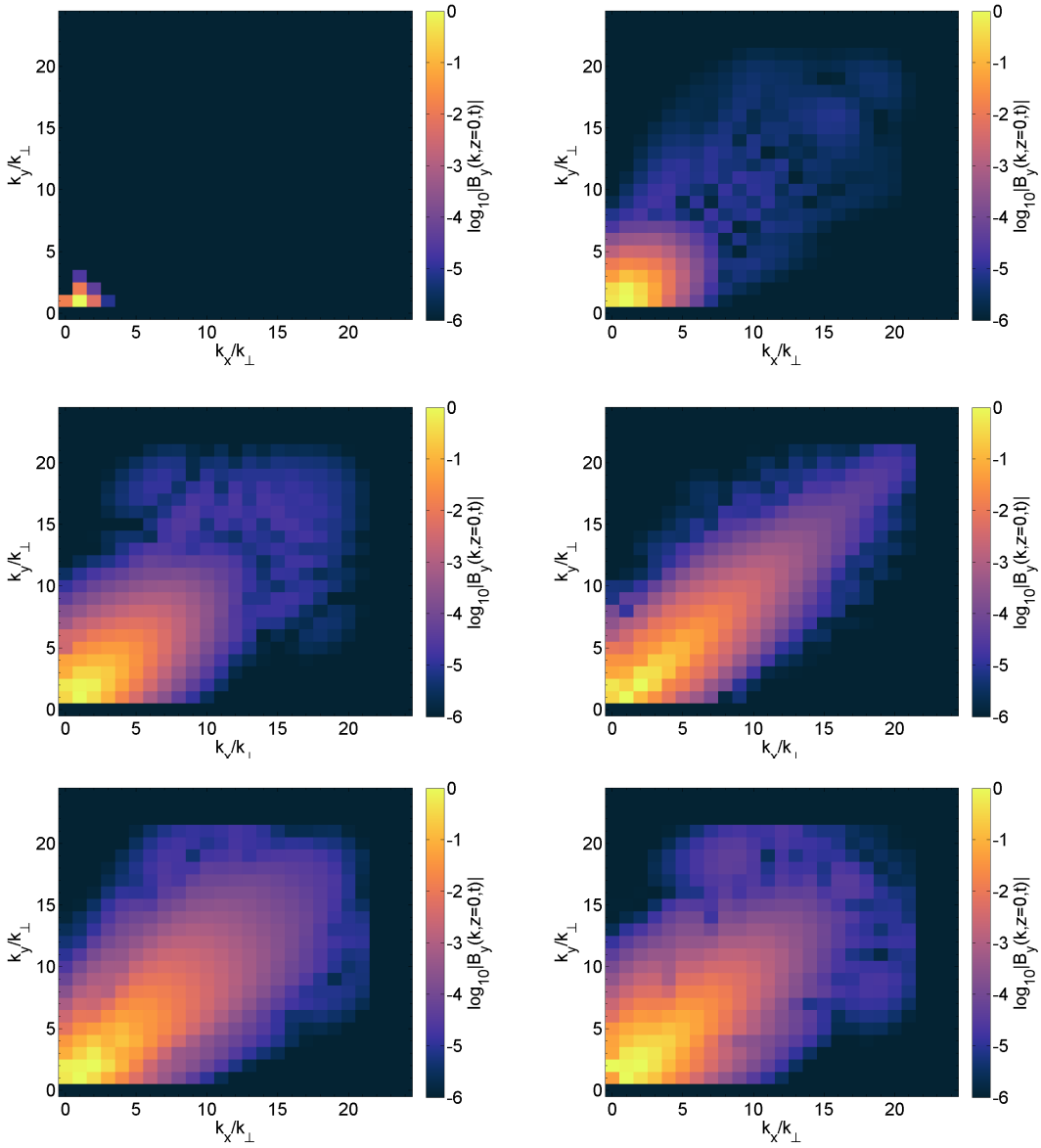

Figure 15: Evolution of $|\widehat{B}_y(\boldsymbol{k})|$ for timestep $n_t = 2,101$ [*row #1*], $n_t = 201,301$ [*row #2*], and $n_t = 401,501$ [*row #3*]. Note logarithmic color axis, and limitation to $k_x, k_y \leq 24k_\perp$.

timesteps	$(k_{1x}, k_{1y}, k_{2x}, k_{2y})$	$\boldsymbol{k}_1 + \boldsymbol{k}_2$	$b^2(\boldsymbol{k}_1, \boldsymbol{k}_2)$
[1,101]	(0,2,2,1)	(2,3)	0.999
	(0,2,2,2)	(2,4)	0.996
	(0,2,0,2)	(0,4)	0.988
	(0,2,3,1)	(3,3)	0.985
	(0,2,1,2)	(1,4)	0.975
	(1,1,0,2)	(1,3)	0.965
	(0,1,0,2)	(0,3)	0.964
	(0,1,3,1)	(3,2)	0.964
	(0,1,2,3)	(2,4)	0.962
	(0,1,3,2)	(3,3)	0.961
	(0,1,2,1)	(2,2)	0.961
	(0,1,2,2)	(2,3)	0.954
	(0,1,1,3)	(1,4)	0.948
	(0,1,1,2)	(1,3)	0.935
	(1,1,0,3)	(1,4)	0.930
	(0,1,1,1)	(1,2)	0.920
[101,201]	(0,2,4,4)	(4,6)	0.970
	(0,2,3,3)	(3,5)	0.965
	(1,1,2,5)	(3,6)	0.965
	(0,2,3,2)	(3,4)	0.964
	(0,2,3,4)	(3,6)	0.963
	(0,2,4,3)	(4,5)	0.961
	(2,2,2,4)	(4,6)	0.959
	(0,2,2,1)	(2,3)	0.955
	(1,1,5,5)	(6,6)	0.954
	(1,1,4,5)	(5,6)	0.954
	(1,1,5,4)	(6,5)	0.952
	(0,2,1,4)	(1,6)	0.951
	(1,1,2,4)	(3,5)	0.951
	(2,2,4,2)	(6,4)	0.951
	(1,1,4,2)	(5,3)	0.951
	(1,1,3,5)	(4,6)	0.949
[201,301]	(1,2,0,3)	(1,5)	0.983
	(0,1,2,2)	(2,3)	0.975
	(2,2,4,4)	(6,6)	0.971
	(0,3,3,2)	(3,5)	0.970
	(2,2,5,5)	(7,7)	0.970
	(0,3,4,3)	(4,6)	0.968
	(2,2,2,5)	(4,7)	0.967
	(0,1,5,5)	(5,6)	0.967
	(0,1,4,4)	(4,5)	0.966
	(3,3,4,4)	(7,7)	0.966
	(2,2,6,6)	(8,8)	0.966
	(0,1,3,3)	(3,4)	0.965
	(0,3,2,3)	(2,6)	0.965
	(0,1,6,6)	(6,7)	0.965
	(2,2,3,6)	(5,8)	0.964
	(2,2,3,3)	(5,5)	0.964

timesteps	$(k_{1x}, k_{1y}, k_{2x}, k_{2y})$	$\boldsymbol{k}_1 + \boldsymbol{k}_2$	$b^2(\boldsymbol{k}_1, \boldsymbol{k}_2)$
[301,401]	(2,2,4,5)	(6,7)	0.998
	(2,2,5,4)	(7,6)	0.998
	(2,2,6,6)	(8,8)	0.997
	(2,2,6,7)	(8,9)	0.996
	(2,2,7,6)	(9,8)	0.995
	(2,2,5,6)	(7,8)	0.995
	(2,2,5,5)	(7,7)	0.995
	(2,2,6,5)	(8,7)	0.995
	(2,2,4,4)	(6,6)	0.995
	(2,2,4,6)	(6,8)	0.994
	(2,2,7,7)	(9,9)	0.994
	(2,2,6,4)	(8,6)	0.994
	(2,2,2,3)	(4,5)	0.990
	(2,2,3,2)	(5,4)	0.990
	(2,2,5,7)	(7,9)	0.990
	(2,3,2,3)	(4,6)	0.988
[401,501]	(2,2,2,2)	(4,4)	0.991
	(0,2,2,1)	(2,3)	0.990
	(2,2,4,4)	(6,6)	0.982
	(1,2,4,2)	(5,4)	0.981
	(2,1,2,4)	(4,5)	0.981
	(0,2,4,2)	(4,4)	0.980
	(0,2,2,3)	(2,5)	0.979
	(0,2,1,4)	(1,6)	0.977
	(0,2,7,4)	(7,6)	0.975
	(2,2,0,4)	(2,6)	0.974
	(2,2,3,2)	(5,4)	0.972
	(2,2,2,3)	(4,5)	0.972
	(0,2,1,3)	(1,5)	0.971
	(2,2,3,5)	(5,7)	0.962
	(0,2,2,2)	(2,4)	0.961
	(2,2,5,3)	(7,5)	0.961
[1,501]	(2,2,7,7)	(9,9)	0.957
	(2,2,2,2)	(4,4)	0.948
	(2,2,7,8)	(9,10)	0.947
	(2,2,6,6)	(8,8)	0.944
	(2,2,8,7)	(10,9)	0.942
	(2,2,8,8)	(10,10)	0.939
	(2,2,5,6)	(7,8)	0.938
	(2,2,6,5)	(8,7)	0.938
	(2,2,4,4)	(6,6)	0.938
	(2,2,6,7)	(8,9)	0.936
	(2,2,7,6)	(9,8)	0.935
	(2,2,5,5)	(7,7)	0.929
	(2,2,5,7)	(7,9)	0.917
	(2,2,7,5)	(9,7)	0.916
	(2,2,4,5)	(6,7)	0.909
	(2,2,5,4)	(7,6)	0.909

Table 3: Greatest 16 values of squared auto-bicoherence $b^2(\boldsymbol{k}_1, \boldsymbol{k}_2)$ over six intervals of AstroGK output, for $B_y(x, y, z = 0, t)$

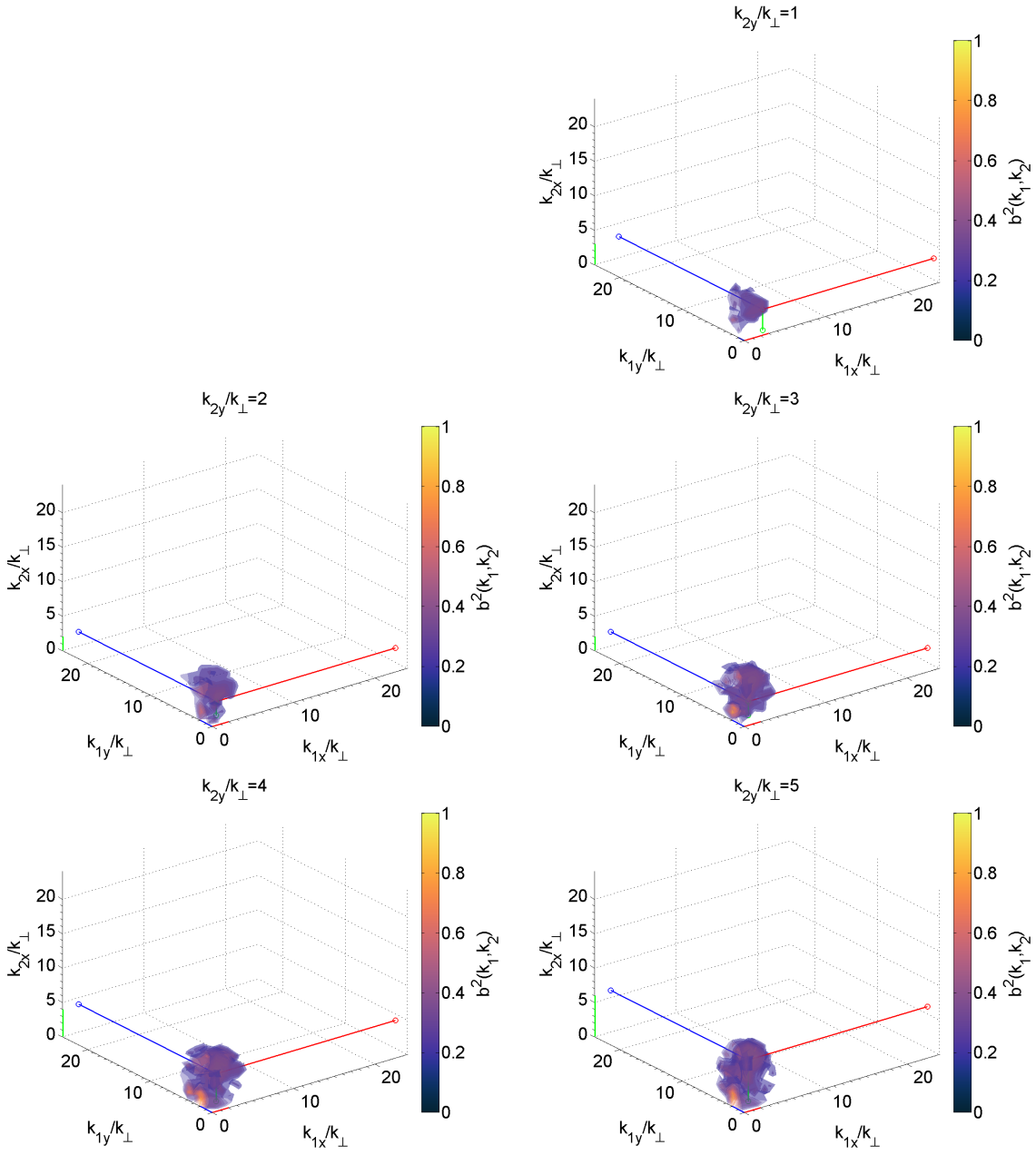

Figure 16: Isosurfaces of squared bicoherence $b^2(\boldsymbol{k}_1, \boldsymbol{k}_2)$ for $n_t = [1, 501]$ and $k_{2y}/k_\perp = [1, 5]$. Note that most peaks involve $\boldsymbol{k}/k_\perp = (2, 2)$; more detailed information is given in Table 3.

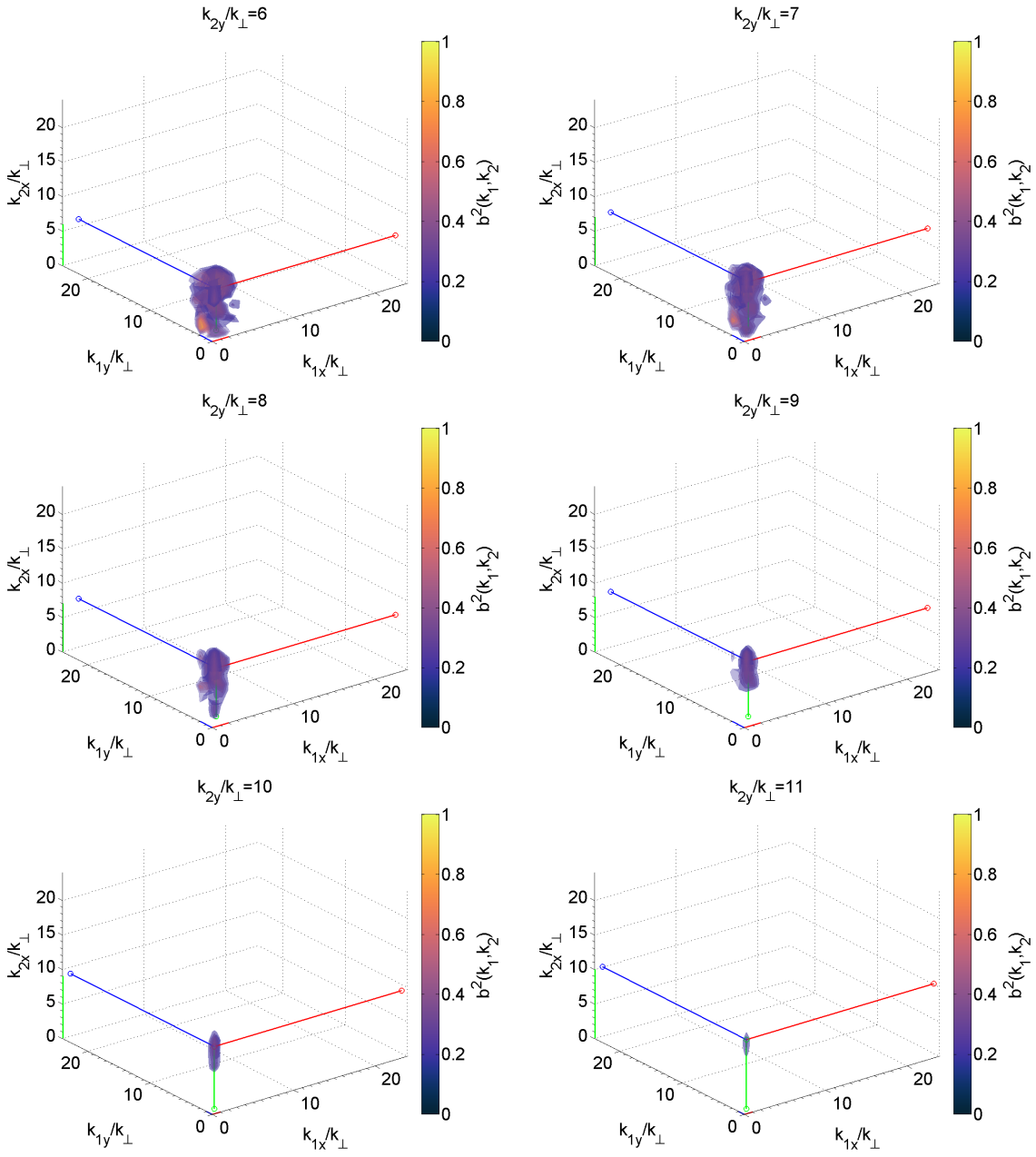

Figure 17: Isosurfaces of squared bicoherence $b^2(\boldsymbol{k}_1, \boldsymbol{k}_2)$ for $n_t = [1, 501]$ and $k_{2y}/k_\perp = [6, 11]$. Note again the appearance of $\boldsymbol{k}/k_\perp = (2, 2)$; see Table 3 for more information.

References

Howes, Gregory G and Kevin D Nielson (2013). "Alfvén wave collisions, the fundamental building block of plasma turbulence. I. Asymptotic solution". In: *Physics of Plasmas* 20(7), p. 072302.

Howes, Gregory G (2016). "The dynamical generation of current sheets in astrophysical plasma turbulence". In: *The Astrophysical Journal Letters* 827(2), p. L28.

Riggs, Gregory Allen (2020). *Interpretations of bicoherence in space & lab plasma dynamics*. West Virginia University.